JACS Au
AN OPEN ACCESS JOURNAL OF THE AMERICAN CHEMICAL SOCIETY

pubs.acs.org/jacsau

Article

pH-Universal Decoupled Water Electrolysis Enabled by Electrocatalytic Hydrogen Gas Capacitive Chemistry

Zhengxin Zhu, Taoli Jiang, Jifei Sun, Zaichun Liu, Zehui Xie, Shuang Liu, Yahan Meng, Qia Peng, Weiping Wang, Kai Zhang, Hongxu Liu, Yuan Yuan, Ke Li, and Wei Chen*

Cite This: *JACS Au* 2023, 3, 488–497

Read Online

ACCESS | Metrics & More | Article Recommendations | Supporting Information

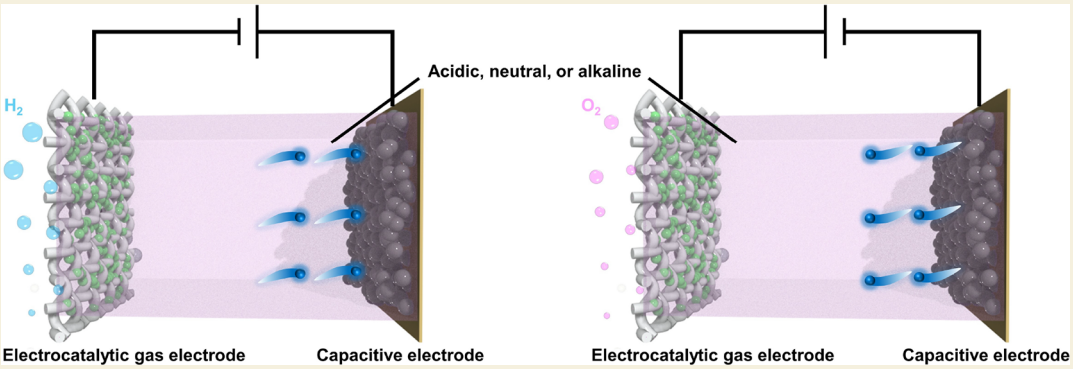

ABSTRACT: In conventional water electrolysis (CWE), the H_2 and O_2 evolution reactions (HER/OER) are tightly coupled, making the generated H_2 and O_2 difficult to separate, thus resulting in complex separation technology and potential safety issues. Previous efforts on the design of decoupled water electrolysis mainly concentrated on multi-electrode or multi-cell configurations; however, these strategies have the limitation of involving complicated operations. Here, we propose and demonstrate a pH-universal, two-electrode capacitive decoupled water electrolyzer (referred to as all-pH-CDWE) in a single-cell configuration by utilizing a low-cost capacitive electrode and a bifunctional HER/OER electrode to separate H_2 and O_2 generation for decoupling water electrolysis. In the all-pH-CDWE, high-purity H_2 and O_2 generation alternately occur at the electrocatalytic gas electrode only by reversing the current polarity. The designed all-pH-CDWE can maintain a continuous round-trip water electrolysis for over 800 consecutive cycles with an electrolyte utilization ratio of nearly 100%. As compared to CWE, the all-pH-CDWE achieves energy efficiencies of 94% in acidic electrolytes and 97% in alkaline electrolytes at a current density of 5 mA cm^{-2}. Further, the designed all-pH-CDWE can be scaled up to a capacity of 720 C in a high current of 1 A for each cycle with a stable HER average voltage of 0.99 V. This work provides a new strategy toward the mass production of H_2 in a facilely rechargeable process with high efficiency, good robustness, and large-scale applications.

KEYWORDS: *decoupling water electrolysis, H_2 production, electrocatalytic H_2, pH-universal, mass production of H_2*

Currently, fossil fuels such as oil, coal, and natural gas are still the major consumed resources in global energy supply.[1,2] However, these non-renewable resources do not comply with the development of a low-carbon society.[3] Hydrogen gas (H_2) has been advocated as a green energy carrier for many chemical transformations compared with fossil fuels due to its high energy density and clean products during utilization.[4−6] In addition, H_2 as an electrocatalytic electrode has recently been developed in rechargeable H_2 battery systems to produce H_2 during the charging process.[7−11] Water electrolysis powered by renewable energy is a sustainable technology for the mass production of H_2 because water is one of the largest reservoirs of H_2 on earth.[12,13] Typically, in conventional water electrolysis (CWE), which involves a H_2 electrode, an oxygen gas (O_2) electrode, and an ion-exchange membrane (IEM), the H_2 evolution reaction (HER) and O_2 evolution reaction (OER) happen simultaneously and thus are tightly coupled.[14,15] The simultaneous H_2 and O_2 generation by the electrocatalytic electrodes are also applied in flow-electrode capacitive deionization systems, which contributes to the improvement of desalination efficiency.[16,17] However, such a compact coupling of H_2 and O_2 is hard to separate, resulting in gas crossover through the

Received: November 14, 2022
Revised: December 15, 2022
Accepted: December 15, 2022
Published: January 24, 2023

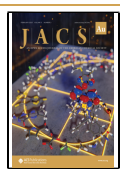

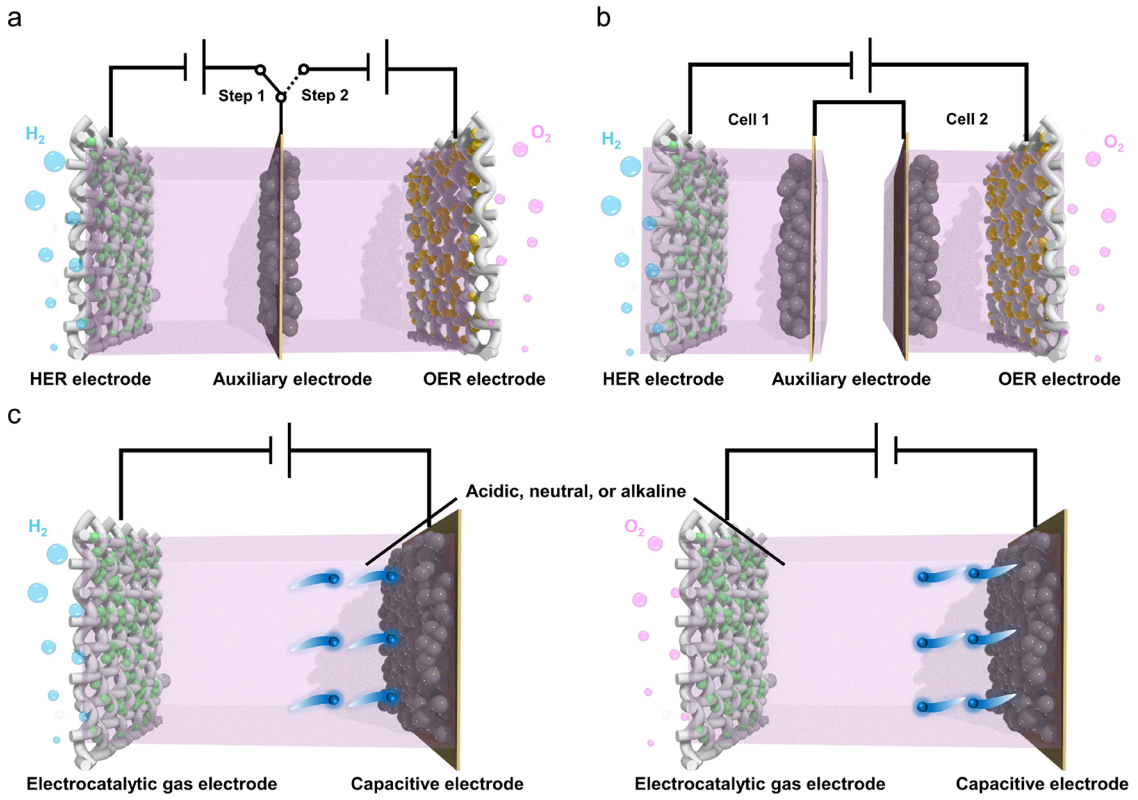

Figure 1. Cell structure and working mechanisms of various decoupled water electrolyzers. (a) Two-step, three-electrode water electrolysis with a frequent on/off switch. (b) Two-cell, four-electrode water electrolysis. (c) Our proposed pH-universal two-electrode electrolytic cell for the decoupling of H_2 and O_2 generation. The electrolytes can be acidic, neutral, and alkaline solutions.

membrane to give rise to hazardous H_2/O_2 mixtures.[18] To overcome these difficulties, it is very crucial to develop novel water electrolysis for decoupling HER and OER.

Recently, the introduction of auxiliary electrodes during water electrolysis allows the decoupling of HER and OER in time or in space.[19−28] For example, Cronin et al. successfully developed a concept of an electron-coupled proton buffer by introducing a soluble silicotungstic acid redox electrode, which can produce hydrogen gas faster than CWE.[29] However, an expensive IEM was employed in the above strategy to restrain the crossover of the soluble redox electrode. To overcome this obstacle, Wang et al. designed a series of inorganic and organic solid-state auxiliary electrodes to temporally decouple HER and OER in an acidic or alkaline water electrolysis process, as illustrated in Figure 1a.[30,31] For instance, a solid-state $Ni(OH)_2$ electrode as an auxiliary electrode was used in an alkaline electrolyte for water electrolysis with the reversible transformation of $Ni(OH)_2/NiOOH$.[30] Moreover, an organic pyrene-4,5,9,10-tetraone (PTO) proton-transfer electrode with a reversible H^+ reaction as an auxiliary electrode was deployed to decouple acidic water electrolysis.[31] However, the above strategies have the limitation of the complicated operation of an frequent on/off switch in three-electrode configurations (a H_2 electrode, an O_2 electrode, and an auxiliary electrode). Meanwhile, Grader et al. introduced a solid-state $NiOOH/Ni(OH)_2$ auxiliary electrode into two-cell water electrolysis, each with a Pt-coated electrode and a $NiOOH/Ni(OH)_2$ electrode, in which the two Pt electrodes were connected to a power source and the nickel electrodes were wired together.[20] The H_2 and O_2 generation can be separated using the $NiOOH/Ni(OH)_2$ electrode, as illustrated in Figure 1b, but in a complicated multi-cell operation. Afterward, they optimized the cell design by changing the water electrolysis process through a two-step electrochemical−chemical cell.[32,33] In the first electrochemical step, H_2 production was achieved by water reduction along with the oxidation of $Ni(OH)_2$ to NiOOH. In the subsequent chemical step, O_2 was liberated by the spontaneous reduction of NiOOH back to $Ni(OH)_2$ at an elevated temperature of ∼95 °C. However, either a $Ni(OH)_2$ or a PTO solid-state electrode is required to comply with strict working conditions for the pH of electrolytes to maintain the stability of auxiliary electrodes, which induces large limitations in the application scenarios for H_2 production.[21,23,30,31,34,35] Therefore, it is highly desirable to develop new strategies to decouple water electrolysis ideally in all pH conditions to make H_2 production much universal and effective.

In this work, a proof-of-concept demonstration of pH-universal decoupled water electrolysis enabled by electrocatalytic H_2 capacitive chemistry, referred to as an all-pH capacitive decoupled water electrolyzer (all-pH-CDWE), is proposed to overcome the abovementioned challenges. The proposal of all-pH-CDWE is inspired by our recently developed electrocatalytic H_2 capacitors, where H_2 is only generated in the charging process for efficient gas separation.[36] Figure 1c shows the structural composition of the designed all-pH-CDWE with a two-electrode configuration of a carbon capacitive electrode and an electrocatalytic gas (H_2 and O_2) electrode, which is fundamentally different from the previous technologies of decoupled water electrolysis by multi-electrode (≥3 electrodes) or multi-cell (≥2 cells) operations (Figure 1a,b).[20,30] Table S1 compares our all-pH-CDWE with other

https://doi.org/10.1021/jacsau.2c00624
JACS Au 2023, 3, 488−497

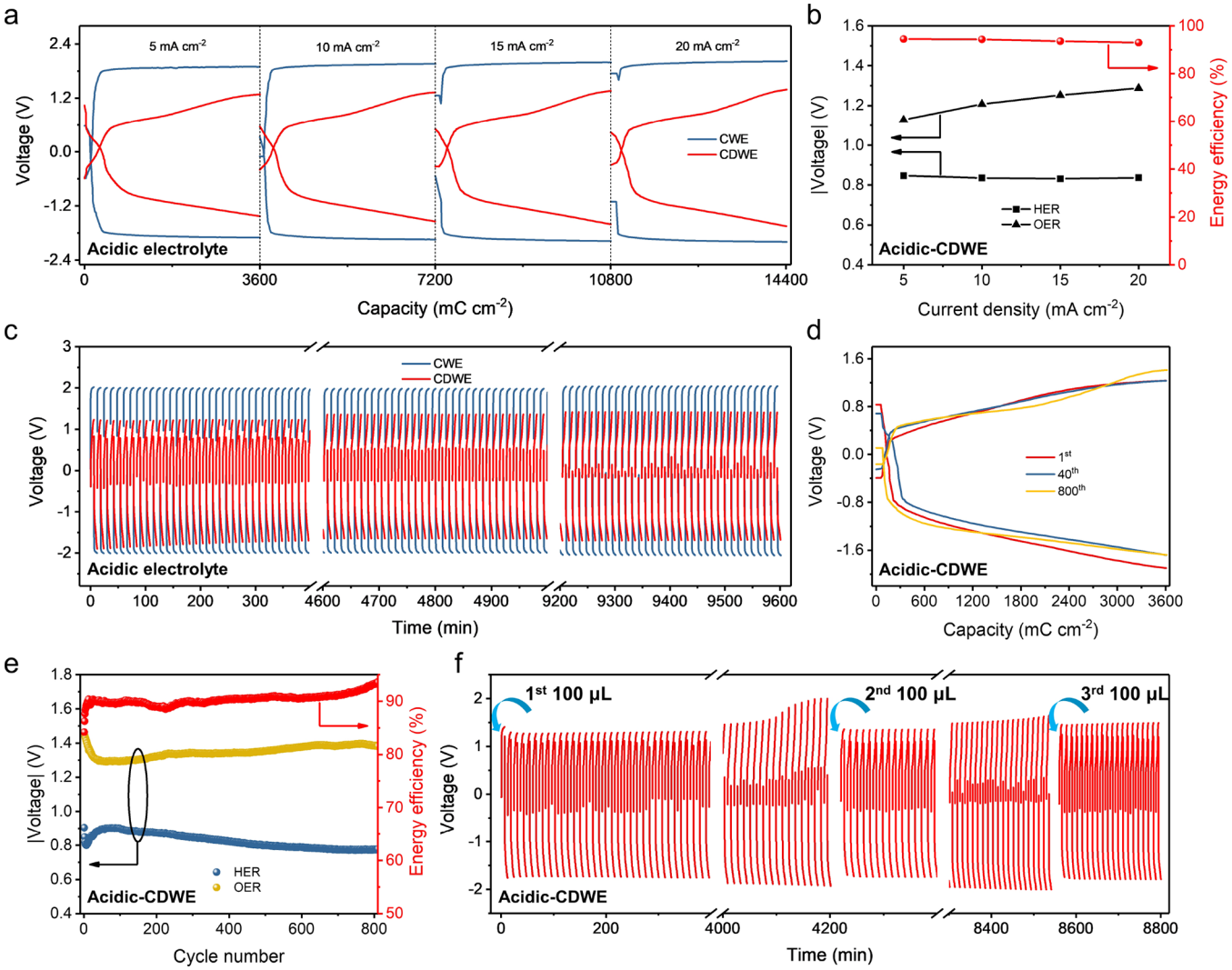

Figure 2. Electrochemical performance of acidic-CDWE in a Swagelok cell. (a) Voltage curves of acidic-CDWE and acidic-CWE at various current densities with an operational capacity of 3600 mC cm^{-2}. (b) HER/OER average voltage and energy efficiency as a function of current density. (c) Voltage curves of acidic-CDWE and acidic-CWE during cycling at a current density of 10 mA cm^{-2} with an operational time of 360 s. (d) Voltage curves at different cycles. (e) HER/OER average voltage and energy efficiency as a function of cycle number. (f) Cycle performance of H_2/O_2 generation by consuming up and repeatedly adding a 100 μL electrolyte into the acidic-CDWE.

reported CWEs and decoupled water electrolyses in terms of cell components, operational modes, and electrochemical performance. It is obvious that in our all-pH-CDWE architecture, the H_2 production involves cathodic H^+ or H_2O reduction and adsorption of anodic anions (SO_4^{2-} in an acidic electrolyte, $H_2PO_4^-/HPO_4^{2-}$ in a neutral electrolyte, or OH^- in an alkaline electrolyte) by the capacitive electrode in pH-universal electrolytes (0−14). The subsequent O_2 production is dependent on the cathodic anion desorption process and the anodic H_2O oxidization reaction. Furthermore, the alternative H_2 and O_2 generation can be cycled with high stability for over 800 consecutive cycles in high electrolyte utilization ratios of nearly 100%. The demonstrated all-pH-CDWE technology shows promises for large-scale H_2 production in a facile and cost-effective pathway.

To verify our designed all-pH-CDWE, a typical Swagelok cell was first designed to decouple water electrolysis with a commercial Pt-coated Ti-mesh electrode for H_2 and O_2 generation and an activated carbon (AC)-coated carbon paper electrode.[8,11,36] As a comparison, CWE with two commercial Pt-coated Ti-mesh electrodes was chosen as the direct water electrolysis. In this all-pH-CDWE, there is a small energy loss by the oxidation and reduction reactions of Pt during the process of alternative H_2 and O_2 generation, which was also reported by previous reports on catalytic gas electrodes.[37−39] As shown in Figure S1, a symmetric capacitor in two AC electrodes was assembled with a capacitance of 1017 mF cm^{-2} at a current density of 5 mA cm^{-2}. Even at a high current density of 20 mA cm^{-2}, a considerable capacitance of 893 mF cm^{-2} was retained (Figure S1), indicating an ultrafast ion adsorption/desorption of the AC electrode.[36,40−43] The water electrolysis performance in the acidic electrolyte was first investigated by chronopotentiometry measurements at various current densities ranging from 5 to 20 mA cm^{-2} with an applied capacity of 3600 mC cm^{-2}, as shown in Figure 2a. In the H_2 generation process, the average voltages of acidic-CDWE are 0.84, 0.84, 0.83, and 0.84 V at current densities of 5, 10, 15, and 20 mA cm^{-2}, respectively, indicating a negligible change of the H_2 generation voltage with the current density and confirming the robustness of the acidic-

https://doi.org/10.1021/jacsau.2c00624
JACS Au 2023, 3, 488−497

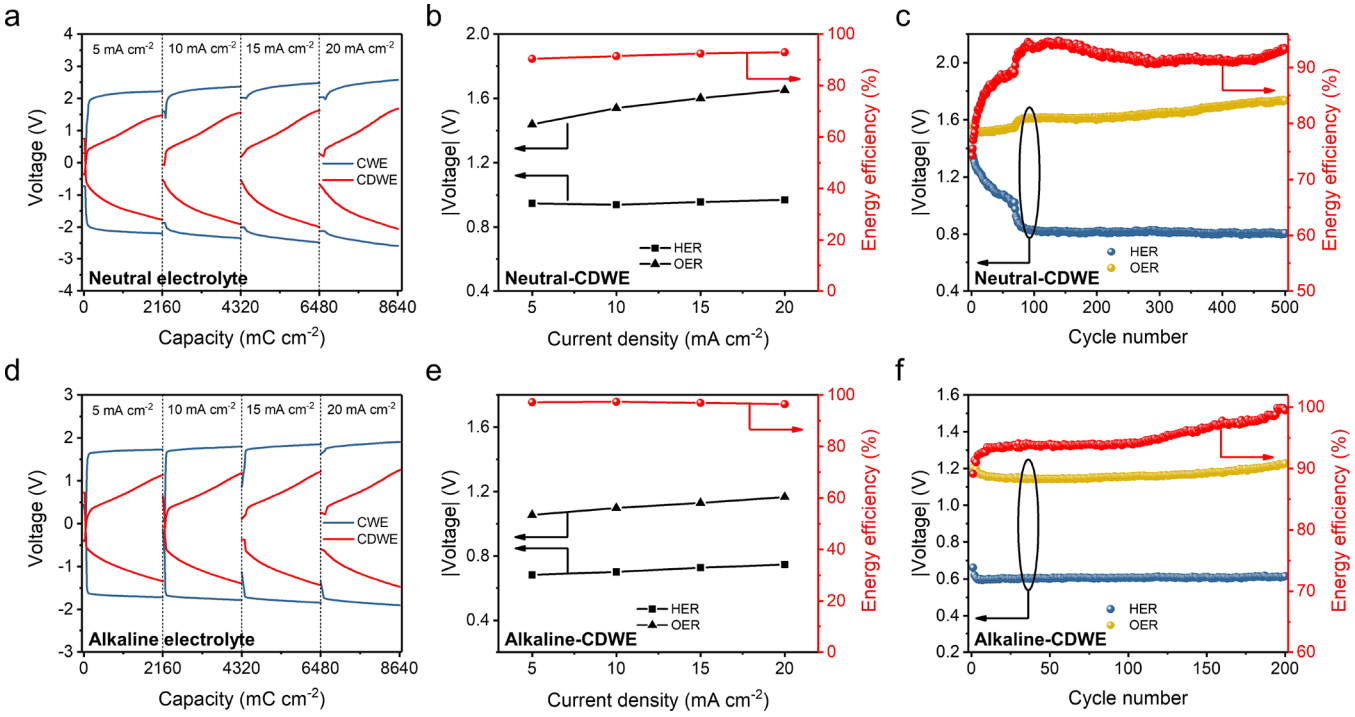

Figure 3. Electrochemical performances of neutral- and alkaline-CDWEs in Swagelok cells. (a) Voltage curves of a neutral-CDWE and neutral-CWE at various current densities with an operational capacity of 2160 mC cm^{-2}. (b) HER/OER average voltage and energy efficiency as a function of current density. (c) HER/OER average voltage and energy efficiency as a function of cycle number at a current density of 10 mA cm^{-2} with an operational time of 216 s. (d) Voltage curves of an alkaline-CDWE and alkaline-CWE at various current densities with an operational capacity of 2160 mC cm^{-2}. (e) HER/OER average voltage and energy efficiency as a function of current density. (f) HER/OER average voltage and energy efficiency as a function of cycle number at a current density of 10 mA cm^{-2} with an operational time of 216 s.

CDWE. In the O_2 generation process, the acidic-CDWE exhibits an increased voltage tendency with average voltages of 1.13, 1.21, 1.25, and 1.29 V at current densities of 5, 10, 15, and 20 mA cm^{-2}, respectively, which is ascribed to the inferior OER performance of the Pt electrode. In addition, the average voltage during H_2 generation process of the acidic-CDWE (0.84 V) is much lower than that of the acidic-CWE (1.98 V) at a large current density of 20 mA cm^{-2} (Figure 2a). Furthermore, the energy efficiency of the acidic-CDWE can be evaluated by comparing its total driving voltage (HER and OER) to that of acidic-CWE, according to a previous report.[30] As shown in Figure 2b, the energy efficiency of the acidic-CDWE with a total driving voltage of 1.97 V is about 94% of that of acidic-CWE with an electrolytic voltage of 1.85 V at a current density of 5 mA cm^{-2}. When the current density increases from 10 to 20 mA cm^{-2}, the energy efficiency of the acidic-CDWE slightly changes from 94 to 93%, which is ascribed to the excellent rate performance of the AC electrode (Figure S1). The achieved energy efficiency is comparable to that of two-step, three-electrode water electrolysis by Wang et al.[21,30] It should be noted that as a notably mature capacitive material, AC not only exhibits high energy efficiency but also delivers an ultralong cycle life, which were demonstrated by the previous literature on an AC electrode-based electrocatalytic hydrogen gas capacitor and electric double-layer capacitors.[36,44−46] These characteristics are important in facilitating the cycling capability of H_2 and O_2 generation. To demonstrate, the cycle performance of H_2 and O_2 generation was investigated with an applied current of 10 mA cm^{-2} for a process time of 360 s. After 800 consecutive cycles (over 160 h), the HER/OER average voltages of acidic-CDWE show a negligible increase, indicating the excellent stability of the H_2 and O_2 generation with a limited electrolyte of 300 μL (Figure 2c). Figure 2c also indicates that the acidic-CDWE delivers a lower operating voltage of H_2 generation than that of acidic-CWE. For the acidic-CDWE, the H_2 generation average voltage slightly decreases and the O_2 generation average voltage slightly increases upon cycling due to the difference between Pt catalytic HER and OER performance (Figure 2d,e). Highly stable energy efficiencies are also observed over the course of 800 round-trip cycles, as shown in Figure 2e. The energy efficiency improves slightly in the initial cycles, which is associated with the activation of the AC electrode.

Further, we tested the water electrolytic performance of the acidic-CDWE with a limited electrolyte volume of 100 μL, as shown in Figure 2f. At an initial amount of 100 μL, the acidic-CDWE is cycled at a constant current density of 10 mA cm^{-2}. The cell delivers stable average voltages for 350 cycles (over 70 h) until the charge voltage increases to 2 V. This indicates that the water solution in our designed electrolytic cell has achieved a high utilization ratio of nearly 100% (the detailed calculation is shown in the Methods section). In the subsequent process, the cell voltage can revert to the original state and continually maintain stable cycling for over another 350 cycles, when an additional 100 μL of the electrolyte was added into the cell. The cycling of the acidic-CDWE with a high electrolyte utilization ratio of nearly 100% can be achieved multiple times by repeatedly adding 100 μL of the electrolyte into the cell as demonstrated in Figure 2f. Figure S2 indicates that the designed acidic-CDWE not only delivers stable H_2 and O_2 generation but also achieves highly efficient utilization of the water solution. The micromorphology, energy-dispersive X-ray

https://doi.org/10.1021/jacsau.2c00624
JACS Au 2023, 3, 488−497

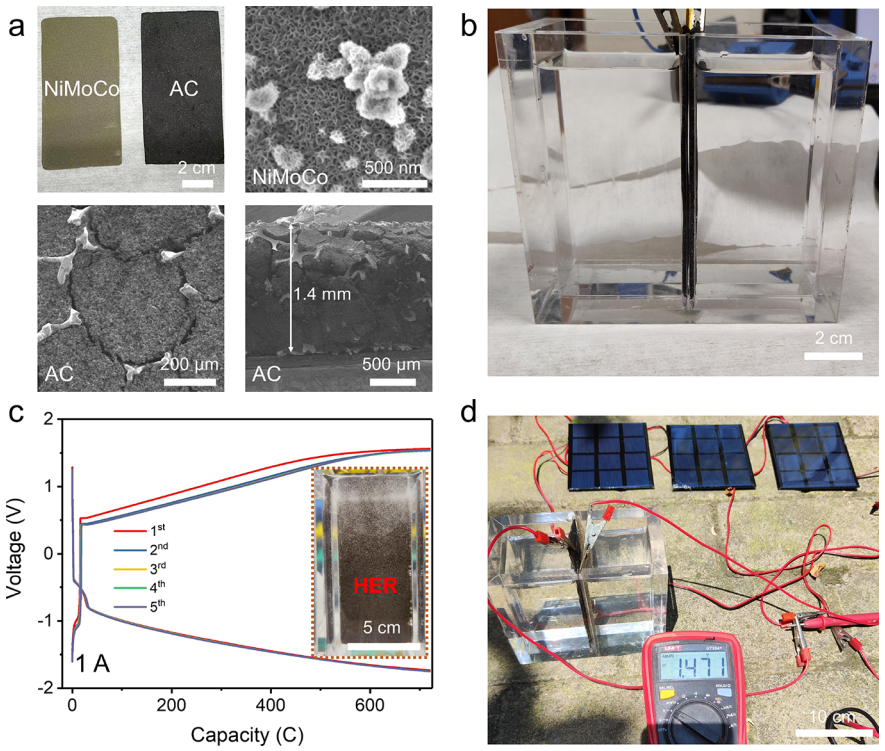

Figure 4. Electrochemical performance of the scaled-up alkaline-CDWE and its practical demonstration. (a) Digital photos and SEM images of the NiMoCo electrode (5 × 10 cm^2) and carbon electrode (5 × 10 cm^2). (b) Digital photo of the scaled-up alkaline-CDWE (10 × 10 × 4.8 cm^3). (c) Voltage curves of the H_2/O_2 generation cycle at a current of 1 A with an operational time of 720 s for each cycle. The inset is the corresponding photo of H_2 generation at a current of 1 A. (d) Photo profile of the HER of photovoltaic-powered water electrolysis under natural sunlight. The rated power, voltage, and current of each solar panel are 1.2 W, 3 V, and 400 mA, respectively.

spectroscopy (EDX), and X-ray photoelectron spectroscopy (XPS) of the AC electrode (Figure S3) show no obvious change after 800 cycles, which confirms the excellent stability of the AC electrode in the acidic-CDWE. Meanwhile, after a long-term cycling test, the phase composition of the Pt electrode displays no obvious change (Figure S4a). The XPS spectra of Pt show that slight oxidization occurred in the Pt electrode after 800 cycles (Figure S4b,c). These characterizations imply the high structural stability of the AC electrode and Pt electrode during the repeated H_2 and O_2 generation processes, proving the robustness of our acidic-CDWE.

To demonstrate pH-universal capability, the water electrolytic performances of the CDWE were further evaluated in neutral and alkaline electrolytes with a Swagelok cell. The feasibility of the AC auxiliary electrode in neutral- and alkaline-CDWEs was verified by chronopotentiometry measurements at different current densities, as shown in Figure 3. A similarly good electrolytic capability was observed in the neutral-CDWE (Figure 3a). As a comparison, the neutral-CDWE delivers lower HER/OER average voltages than the neutral-CWE. Figure 3b reveals that the HER voltage and energy efficiency of neutral-CDWE at 5 mA cm^{-2} are 0.95 V and 90%, respectively. The neutral-CDWE investigated at the other current densities of 10, 15, and 20 mA cm^{-2} further illustrates the operational flexibility of this electrolyzer (Figure 3b). The cycle performance of the H_2 and O_2 generation was investigated with an applied current density of 10 mA cm^{-2} and a process time of 216 s for 500 cycles. After 100 consecutive cycles of this electrolytic process, the HER average voltage tends to stabilize at ∼0.8 V with an energy efficiency of ∼90%, demonstrating the excellent stability of the alternating H_2 and O_2 generation in the neutral-CDWE (Figure 3c and Figure S5). In addition, the alkaline-CDWE delivers a very low HER average voltage of 0.68 V, a cell average voltage of 1.74 V, and a high energy efficiency of 97% at a current density of 5 mA cm^{-2} (Figure 3d,e), which are superior to those from the previous literature on decoupling water electrolysis.[29,30] When the current densities increase to 10, 15, and 20 mA cm^{-2}, the HER average voltages can remain as 0.7, 0.73, and 0.75 V, respectively (Figure 3e). Furthermore, the alkaline-CDWE delivers a lower operational voltage than alkaline-CWE (Figure 3d). The alkaline-CDWE also shows high stability in alkaline water electrolysis for over 200 cycles (Figure 3f and Figure S6). Therefore, it can be concluded that the strategy of the two-electrode design could decouple pH-universal water electrolysis with excellent activity and stability, which further verified the operational flexibility of this all-pH-CDWE with the potential to be applied broadly in the water electrolysis industry.

Based on the above analysis, to further demonstrate the advances and practicality of this novel CDWE for large-scale application in decoupling of H_2 and O_2, we amplified the electrolytic cell by employing a low-cost gas electrode in the CDWE. Accordingly, we took inspiration from the chloride corrosion of metal to prepare a low-cost bifunctional HER/OER electrocatalyst of NiMoCo in alkaline electrolytes.[47] The facilely prepared NiMoCo catalyst exhibited excellent performances toward water splitting with overpotentials of 108 mV at a current density of 20 mA cm^{-2} for HER and 330 mV (20 mA cm^{-2}) for OER, better than those of nickel foam and noble metal Pt (Figure S7). In addition, the NiMoCo catalyst was stable for more than 100 h at a constant current density of 50

https://doi.org/10.1021/jacsau.2c00624
JACS Au 2023, 3, 488−497

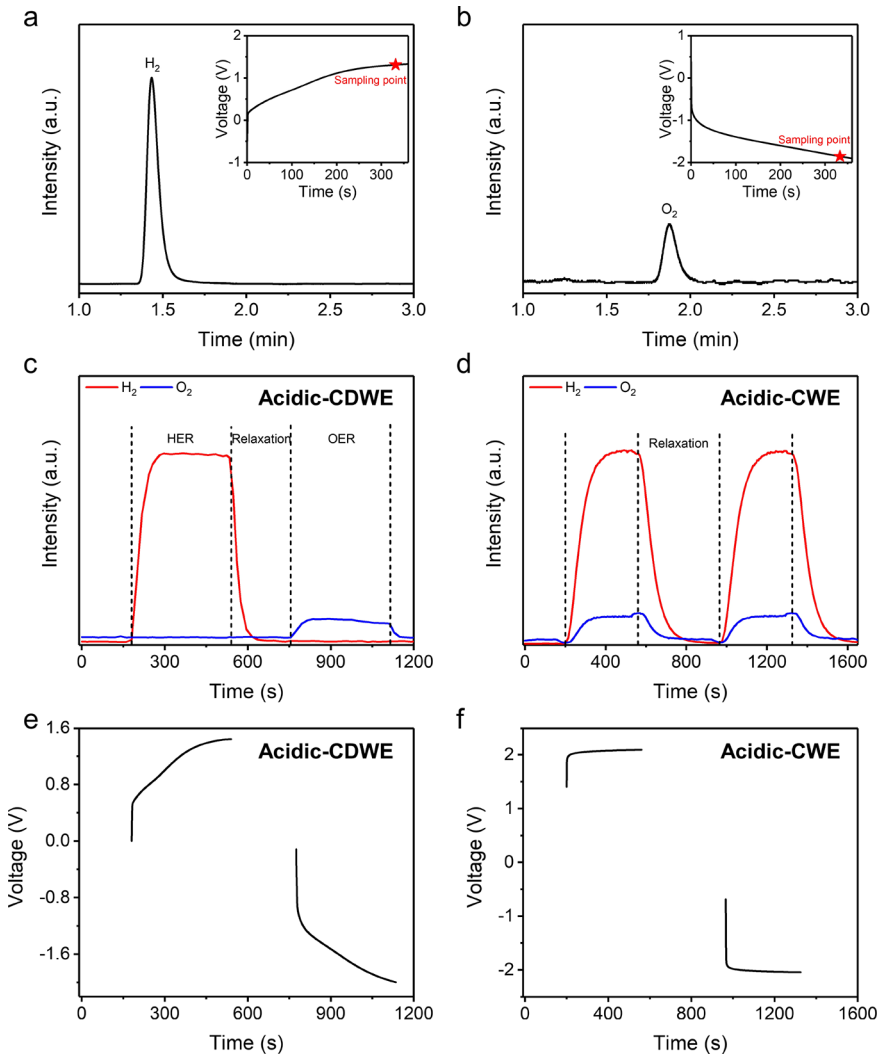

Figure 5. Purity analysis of the generated H_2/O_2 in the CDWE. Gas chromatography for (a) HER and (b) OER. The insets show the corresponding voltage curves of H_2 and O_2 generation by water electrolysis, where the asterisk represents the sampling point. In situ DEMS curves of (c) the acidic-CDWE and (d) acidic-CWE for H_2 evolution (red line) and O_2 evolution (blue line) in the total water electrolysis process at an applied current density of 10 mA cm^{-2} for 360 s. Voltage curves of (e) the acidic-CDWE and (f) acidic-CWE corresponding to the in situ DEMS tests.

mA cm^{-2} toward HER and OER (Figure S8), which is important toward long-term overall water splitting. When the NiMoCo catalyst was used as the electrode for the overall water-splitting device, a current density of 20 mA cm^{-2} could be observed at an applied potential of 1.66 V, which is superior to that of the Pt catalyst (1.95 V) (Figure S9).

To test the feasibility of the electrolytic cell, a scaled-up alkaline-CDWE was constructed with a low-cost NiMoCo-coated nickel foam gas electrode (5 × 10 cm^2), an AC-coated nickel foam electrode (5 × 10 cm^2), and a poly(methyl methacrylate) (PMMA) box with a volume of 0.48 L (10 × 10 × 4.8 cm^3), as shown in Figure 4a. The morphology of the NiMoCo catalyst was observed as nanosheet arrays growing on nickel foam (Figure 4a). In addition, nickel-foam-supported AC particles were used as the active material to prepare a dense and thick carbon electrode with a thickness of 1.4 mm and a capacity of 720 C, as shown in Figure 4a. The two electrode plates were fixed upright and parallel with each other with a gap of 1 mm (Figure 4b). The electrode plates were put inside the PMMA box, and then a 2 M KOH alkaline electrolyte of 380 mL was added into this box. The testing results demonstrate that when the scaled-up alkaline-CDWE was cycled at an applied current of 1 A and an operational time of 720 s, the water electrolytic process stably produced H_2 and O_2 in several consecutive cycles (Figure 4c). Highly stable HER/OER average voltages of 0.99/1.35 V were also observed over the course of several round-trip cycles. The micromorphology and XPS spectra of the AC electrode also show no obvious change after cycles in the scaled-up alkaline-CDWE, which confirms the excellent stability of the AC electrode in large-scale water electrolysis (Figure S10). As shown in Figure S11, the energy efficiency of the scaled-up alkaline-CDWE using a NiMoCo-coated nickel foam gas electrode is 80% as compared to the alkaline-CWE counterpart. It is noticed that the energy efficiency can be further enhanced if optimized AC electrodes are employed. The corresponding photo profile of large H_2 bubbles in the scaled-up alkaline-CDWE at a current of 1 A is shown in the inset of Figure 4c. The video evidence also clearly demonstrates the separated H_2 and O_2 generation in the amplified electrolyzer (Videos S1 and S2, respectively). In addition, we constructed a photovoltaic-powered water electrolysis device that could directly convert water and

https://doi.org/10.1021/jacsau.2c00624
JACS Au 2023, 3, 488−497

sunlight into green H_2 without a membrane, as shown in Figure 4d. The working voltage of HER in the photovoltaic-powered water electrolysis under natural sunshine is about 1.47 V, as displayed in the photo profile (Figure 4d) and the video for H_2 generation (Video S3).

We carried out additional experiments by taking the acidic-CDWE as a typical example to characterize the decoupled water electrolyzers. The photo profiles of H_2 and O_2 generation are shown in Figure S12 to confirm the decoupled characteristics of the acidic-CDWE. It is clearly observed that a large number of bubbles were only produced on the gas electrode, while no bubble was generated on the AC electrode (Figure S12c,d). In addition, the video record confirmed the directly separated H_2 and O_2 generation (Videos S4 and S5). The purity of the H_2 and O_2 produced by decoupling water electrolysis was evaluated by ex situ gas chromatography (GC) and in situ differential electrochemical mass spectrometry (DEMS). The GC and corresponding chronopotentiometry data of voltage curves for H_2 and O_2 generation are shown in Figure 5a,b, respectively. As displayed in Figure 5a, the recorded data showed that only H_2 was detected, indicating no O_2 generation during the HER process. After the charging process, a rest step of 20 min was performed to remove the produced H_2 in the system. Then, O_2 was detected by GC analysis during the subsequent discharging process with no H_2 production (Figure 5b). The results indicated the effectiveness of the capacitive decoupling water electrolysis for the production of high-purity H_2 and O_2.

In addition, in situ DEMS was used to analyze the process of gas production by decoupled water electrolysis at a constantly applied current density of 10 mA cm^{-2}. The obtained in situ DEMS and the corresponding chronopotentiometry data of the acidic-CDWE are given in Figure 5c,e, respectively. As shown in Figure 5c, in parallel with the beginning of charging, H_2 evolution was detected in the online analysis record, whereas O_2 remained at the background level, indicating no O_2 generation during the charging process. After the end of charging, purging with a high-purity N_2 stream was performed for a few minutes to eliminate the remaining H_2 in the system. Then, O_2 evolution was observed in the online analysis record of in situ DEMS during the discharging process but without any H_2 evolution. As a comparison, in situ DEMS and the corresponding chronopotentiometry data of acidic-CWE are shown in Figure 5d,f, respectively. In contrast, H_2 and O_2 evolution were simultaneously observed in the online analysis record, which indicates that H_2 and O_2 generation in acidic-CWE cannot be decoupled. The above ex situ GC and in situ DEMS proved the effectiveness and robustness of the developed capacitive decoupled water electrolyzers as an advanced H_2 and O_2 production and separation technology.

In summary, we have successfully designed and demonstrated a novel all-pH-CDWE in a two-electrode single-cell configuration by utilizing a low-cost capacitive electrode and an electrocatalytic gas electrode for decoupling water electrolysis. The experimental analysis revealed that the interval generation of H_2 and O_2 can be achieved simply by reversing the current polarity of the all-pH-CDWE, which can be cycled with high stability over 800 consecutive cycles in a high electrolyte utilization ratio of nearly 100%. As compared to the driving voltage of CWE, the all-pH-CDWE showed high energy efficiencies of 94% in the acidic-CDWE and 97% in the alkaline-CDWE at a current density of 5 mA cm^{-2}. Ex situ GC and in situ DEMS tests were conducted to confirm the high purity of the decoupling-generated H_2 and O_2. This designed all-pH-CDWE in a highly rechargeable process can be scaled up and well applied in practical water electrolysis to facilitate the utilization of renewable energy resources to generate H_2 in mass production.

METHODS

Fabrication of a Low-Cost NiMoCo Bifunctional Catalyst

Prior to the synthesis of the NiMoCo electrode, a 5 × 10 cm^2 nickel foam (NF) was ultrasonicated with HCl (1 M), acetone, and ethanol for 5 min to ensure that there was no oxide or other purities on the surface. The synthesis of a low-cost NiMoCo bifunctional catalyst was modified on the basis of a previous report.[47] Specifically, a piece of NF was put into a beaker containing NaCl (0.5 M), $CoCl_2{\cdot}6H_2O$ (1 mM), and $MoCl_5$ (1 mM) solutions. Then, the beaker was frequently stirred for 12 h to ensure that the surface of NF can be completely reacted. Finally, the resulting catalyst-coated NF was dried naturally after washing.

Electrode Preparation

For the AC electrode, commercial AC (YEC-8, Fuzhou Yihuan Carbon, Ltd.), acetylene black (MTI), and poly(vinylidene fluoride) (MTI) were well mixed at a weight ratio of 8:1:1 to form a homogeneous slurry by adding the solvent *N*-methylpyrrolidone (Aladdin). After that, the slurry was coated onto carbon paper (Fuel cell store, USA) and formed a dense film with an activated mass loading of ∼15 mg cm^{-2}. For the scaled-up experiment, the AC slurry was injected into an NF with an activated mass loading of ∼80 mg cm^{-2}.

Water Electrolysis Investigation

In a beaker cell, galvanostatic measurements of the all-pH-CDWE with an AC electrode and a commercial Pt-coated Ti mesh (Suzhou Shure Tai Industrial Technology Co. Ltd.) as the gas electrode were carried out on a Landhe battery-testing instrument, a Neware battery-testing system, and a VMP-3 multi-channel electrochemical workstation. The all-pH-CDWE was designed in a Swagelok cell that was used to test H_2 batteries previously,[8,11,36] which can effectively collect H_2 and O_2. The typical Swagelok cell was made of an AC electrode, a Pt gas electrode, and a glass fiber (GF/D, Whatman) separator with a certain amount of electrolyte. The Swagelok device was made up of stainless-steel inlet and outlet valves with a Klein flange in a polytetrafluoroethylene-centered O-ring that was assembled with a clamp, as shown in Figure S13. The electrolyte solutions were 100 or 300 μL of 0.5 M H_2SO_4 for the acidic-CDWE, 200 μL of 1 M KH_2PO_4/K_2HPO_4 (phosphate buffer solution) for the neutral-CDWE, and 200 μL of 2 M KOH for the alkaline-CDWE. All experiments were performed at room temperature.

Calculation of Utilization of the Electrolyte

For the acidic-CDWE, the amount of transferred charge is calculated by the equation $n = It/F$, where I is the current density, t is the electrolytic time, and F is the Faraday constant. According to the reaction of water splitting, $2H_2O \rightarrow 2H_2 + O_2$, the amount of transferred charge is twice as much as that of the consumed water. Therefore, the theoretical volume of the consumed water can be calculated by the equation $V_T = 0.5ItM/F\rho$, where M is the molecular mass of water and ρ is the density of water.

Calculation of Energy Efficiency of the CDWE

For the CDWE, the energy efficiency (EE) can be calculated by the equation $EE = E_{CWE}/E_{CDWE}$, where E_{CWE} is the input energy of CWE and E_{CDWE} is the input energy of the CDWE for the overall water splitting. According to the equation $E = C \times U$, where C is the capacity of the cells, the EE of the CDWE can be expressed as $EE = U_{CWE}/(U_{HER} + U_{OER})$, where U_{HER} is the average voltage in the H_2 generation process of the CDWE, U_{OER} is the average voltage in the O_2 generation process of the CDWE, and U_{CWE} is the average voltage of the CWE.

https://doi.org/10.1021/jacsau.2c00624
JACS Au 2023, 3, 488−497

Gas Product Analysis

Gas products from the water electrolytic cell during HER and OER were detected and analyzed using ex situ GC (GC-2014c) and in situ DEMS (HPR-40 DEMS). The water electrolytic cell was sealed in the Swagelok cell, which was connected to a GC-2014c by two tubes as the gas inlet and outlet (Figure S14). High-purity Ar was used as the carrier gas and purified gas. Before testing, the sealed electrolytic cell was purified with Ar gas at a flow rate of 5 mL min^{-1} for 20 min to eliminate the air inside the cell. After that, HER and OER were performed using an SP-150 single-channel electrochemical workstation (BioLogic) with an applied current density of 20 mA (2 cm^2) in an acidic electrolyte. After about 5.5 min, the H_2 produced in the charging process was collected and analyzed by the GC instrument. Using the same method, a high-purity Ar gas stream was purged again for 20 min to blow out the H_2 in the cell. A current density of 20 mA (2 cm^2) was applied for 5.5 min, and the O_2 produced in the discharging process was also collected and analyzed by the GC instrument. In addition, the mass spectrometer was connected to the Swagelok water electrolytic cell with two tubes as the gas inlet and outlet (Figure S14). A high-purity N_2 gas stream was used as the purging gas before electrolysis and the carrier gas during the electrolysis process. The gas flows were controlled to be 4 mL min^{-1}. Before the online gas analysis, the system was purged with a high-purity N_2 stream for a few minutes. HER and OER were performed using a Chenhua electrochemical workstation with an applied current density of 20 mA (2 cm^2) in the acidic-CDWE. The operational duration of the charge was set to be 6 min. After the end of the charging step, purging with a high-purity N_2 stream was performed for a few minutes to eliminate any remaining H_2 in the system. Then, the discharging step was started and continued until the cell voltage sharply increased. The experiment was completed when almost no remaining O_2 in the electrolytic cell can be detected.

Physicochemical Characterizations

The morphologies of the AC electrodes and the NiMoCo catalytic electrodes were characterized with a scanning electron microscope (SEM) instrument (Hitachi 8220). Energy-dispersive X-ray spectroscopy was collected by the SEM instrument. Powder X-ray diffraction (PXRD) patterns were collected with a Philips X'Pert Pro Super X-ray diffractometer equipped with graphite monochromatized Cu K_α radiation. X-ray photoelectron spectroscopy (XPS) measurements of the carbon electrode and Pt electrode were performed with an ESCALAB 250Xi.

■ ASSOCIATED CONTENT

Supporting Information

The Supporting Information is available free of charge at https://pubs.acs.org/doi/10.1021/jacsau.2c00624.

(Figure S1) Charge/discharge curves and rate capacitance of the AC symmetric capacitor; (Figure S2) voltage curves of the acidic-CDWE in different cycles when repeatedly adding 100 μL electrolyte into the cell; (Figure S3) SEM images, EDX analyses, and XPS spectra of the fresh AC electrode and the AC electrode after 800 cycles in an acidic-CDWE; (Figure S4) XRD patterns and XPS spectra of the Pt electrode in the initial state and after 800 cycles in an acidic-CDWE; (Figures S5 and S6) voltage curves of the neutral-CDWE and alkaline-CDWE during cycling; (Figure S7) HER and OER performances of Ni foam, PtTi, and NiMoCo catalysts; (Figure S8) HER and OER stability tests of the NiMoCo catalyst; (Figure S9) polarization curves of NiMoCo and Pt catalysts for overall water splitting; (Figure S10) SEM image and XPS spectrum of the AC electrode after cycling in the scaled-up alkaline-CDWE; (Figure S11) voltage curves of CWE cycles in the scaled-up electrolytic cell; (Figure S12) characterization of the acidic-CDWE in a beaker testing cell; (Figures S13 and S14) digital photographs of the testing Swagelok device of the all-pH-CDWE and the all-pH-CDWE connected to the DEMS device; (Table S1) comparison of different water electrolysis technologies; (Table S2) EDX elemental contents of the fresh AC electrode and AC electrode after 800 cycles (PDF)

(Video S1) H_2 generation in the scaled-up alkaline-CDWE (MP4)

(Video S2) O_2 generation in the scaled-up alkaline-CDWE (MP4)

(Video S3) H_2 generation in the photovoltaic-powered water electrolysis device (MP4)

(Video S4) H_2 generation in the acidic-CDWE (MP4)

(Video S5) O_2 generation in the acidic-CDWE (MP4)

■ AUTHOR INFORMATION

Corresponding Author

Wei Chen − *Department of Applied Chemistry, School of Chemistry and Materials Science, Hefei National Research Center for Physical Sciences at the Microscale, University of Science and Technology of China, Hefei, Anhui 230026, China*; orcid.org/0000-0002-8018-4529; Email: weichen1@ustc.edu.cn

Authors

Zhengxin Zhu − *Department of Applied Chemistry, School of Chemistry and Materials Science, Hefei National Research Center for Physical Sciences at the Microscale, University of Science and Technology of China, Hefei, Anhui 230026, China*

Taoli Jiang − *Department of Applied Chemistry, School of Chemistry and Materials Science, Hefei National Research Center for Physical Sciences at the Microscale, University of Science and Technology of China, Hefei, Anhui 230026, China*

Jifei Sun − *Department of Applied Chemistry, School of Chemistry and Materials Science, Hefei National Research Center for Physical Sciences at the Microscale, University of Science and Technology of China, Hefei, Anhui 230026, China*; orcid.org/0000-0002-0877-900X

Zaichun Liu − *Department of Applied Chemistry, School of Chemistry and Materials Science, Hefei National Research Center for Physical Sciences at the Microscale, University of Science and Technology of China, Hefei, Anhui 230026, China*

Zehui Xie − *Department of Applied Chemistry, School of Chemistry and Materials Science, Hefei National Research Center for Physical Sciences at the Microscale, University of Science and Technology of China, Hefei, Anhui 230026, China*

Shuang Liu − *Department of Applied Chemistry, School of Chemistry and Materials Science, Hefei National Research Center for Physical Sciences at the Microscale, University of Science and Technology of China, Hefei, Anhui 230026, China*

Yahan Meng − *Department of Applied Chemistry, School of Chemistry and Materials Science, Hefei National Research Center for Physical Sciences at the Microscale, University of Science and Technology of China, Hefei, Anhui 230026, China*

https://doi.org/10.1021/jacsau.2c00624
JACS Au 2023, 3, 488−497

Qia Peng − *Department of Applied Chemistry, School of Chemistry and Materials Science, Hefei National Research Center for Physical Sciences at the Microscale, University of Science and Technology of China, Hefei, Anhui 230026, China*

Weiping Wang − *Department of Applied Chemistry, School of Chemistry and Materials Science, Hefei National Research Center for Physical Sciences at the Microscale, University of Science and Technology of China, Hefei, Anhui 230026, China*

Kai Zhang − *Department of Applied Chemistry, School of Chemistry and Materials Science, Hefei National Research Center for Physical Sciences at the Microscale, University of Science and Technology of China, Hefei, Anhui 230026, China*

Hongxu Liu − *Department of Applied Chemistry, School of Chemistry and Materials Science, Hefei National Research Center for Physical Sciences at the Microscale, University of Science and Technology of China, Hefei, Anhui 230026, China*

Yuan Yuan − *Department of Applied Chemistry, School of Chemistry and Materials Science, Hefei National Research Center for Physical Sciences at the Microscale, University of Science and Technology of China, Hefei, Anhui 230026, China*

Ke Li − *Department of Applied Chemistry, School of Chemistry and Materials Science, Hefei National Research Center for Physical Sciences at the Microscale, University of Science and Technology of China, Hefei, Anhui 230026, China*

Complete contact information is available at: https://pubs.acs.org/10.1021/jacsau.2c00624

Author Contributions

CRediT: **Zhengxin Zhu** data curation, investigation, methodology, project administration, writing-original draft, writing-review & editing; **Taoli Jiang** visualization; **Jifei Sun** visualization; **Zaichun Liu** visualization; **Zehui Xie** visualization; **Shuang Liu** visualization; **Yahan Meng** visualization; **Qia Peng** visualization; **Weiping Wang** visualization; **Hongxu Liu** visualization; **Yuan Yuan** visualization; **Ke Li** visualization; **Wei Chen** funding acquisition, project administration, writing-original draft, writing-review & editing.

Notes

The authors declare the following competing financial interest(s): A patent based on this work was filed on June 3, 2021.

■ ACKNOWLEDGMENTS

This research work was supported by startup funds from the USTC (Grant No. KY2060000150) and the Fundamental Research Funds for the Central Universities (WK2060000040). We thank the support from the USTC Center for Micro and Nanoscale Research and Fabrication.

■ REFERENCES

(1) Turner, J. A. A Realizable Renewable Energy Future. *Science* **1999**, *285*, 687−689.

(2) Zhu, Z.; Jiang, T.; Ali, M.; Meng, Y.; Jin, Y.; Cui, Y.; Chen, W. Rechargeable Batteries for Grid Scale Energy Storage. *Chem. Rev.* **2022**, *122*, 16610−16751.

(3) Wang, M.; Zheng, X.; Zhang, X.; Chao, D.; Qiao, S.-Z.; Alshareef, H. N.; Cui, Y.; Chen, W. Opportunities of Aqueous Manganese-Based Batteries with Deposition and Stripping Chemistry. *Adv. Energy Mater.* **2021**, *11*, 1704378.

(4) Ball, M.; Weeda, M. The hydrogen economy − Vision or reality? *Int. J. Hydrogen Energy* **2015**, *40*, 7903−7919.

(5) Wei, D.; Sang, R.; Moazezbarabadi, A.; Junge, H.; Beller, M. Homogeneous Carbon Capture and Catalytic Hydrogenation: Toward a Chemical Hydrogen Battery System. *JACS Au* **2022**, *2*, 1020−1031.

(6) Wang, Y.; Jin, F.; Zeng, X.; Ma, C.; Wang, F.; Yao, G.; Jing, Z. Catalytic activity of Ni_3S_2 and effects of reactor wall in hydrogen production from water with hydrogen sulphide as a reducer under hydrothermal conditions. *Appl. Energy* **2013**, *104*, 306−309.

(7) Turner, J. A. Sustainable Hydrogen Production. *Science* **2004**, *305*, 972−974.

(8) Chen, W.; Li, G.; Pei, A.; Li, Y.; Liao, L.; Wang, H.; Wan, J.; Liang, Z.; Chen, G.; Zhang, H.; et al. A manganese−hydrogen battery with potential for grid-scale energy storage. *Nat. Energy* **2018**, *3*, 428−435.

(9) Zhu, Z.; Meng, Y.; Cui, Y.; Chen, W. An Ultrastable Aqueous Iodine-Hydrogen Gas Battery. *Adv. Funct. Mater.* **2021**, *31*, 2101024.

(10) Zhu, Z.; Meng, Y.; Yin, Y.; Liu, Z.; Jiang, T.; Peng, Q.; Yin, T.; Li, M.; Chen, W. High performance aqueous Prussian blue analogue-hydrogen gas hybrid batteries. *Energy Storage Mater.* **2021**, *42*, 464−469.

(11) Zhu, Z.; Wang, W.; Yin, Y.; Meng, Y.; Liu, Z.; Jiang, T.; Peng, Q.; Sun, J.; Chen, W. An Ultrafast and Ultra-Low-Temperature Hydrogen Gas-Proton Battery. *J. Am. Chem. Soc.* **2021**, *143*, 20302−20308.

(12) Berger, A.; Segalman, R. A.; Newman, J. Material requirements for membrane separators in a water-splitting photoelectrochemical cell. *Energy Environ. Sci.* **2014**, *7*, 1468−1476.

(13) Jiang, X.; Liu, Q.; Cheng, C.; Xing, F.; Chen, C.; Huang, C. In situ photodeposition of metalloid Ni2P co-catalyst on Mn0.5Cd0.5S for enhanced photocatalytic H2 evolution with visible light. *Int. J. Hydrogen Energy* **2021**, *46*, 5197−5206.

(14) Paul, A.; Symes, M. D. Decoupled electrolysis for water splitting. *Curr. Opin. Green Sustainable Chem.* **2021**, *29*, 100453.

(15) Chen, G.; Wang, T.; Zhang, J.; Liu, P.; Sun, H.; Zhuang, X.; Chen, M.; Feng, X. Accelerated Hydrogen Evolution Kinetics on NiFe-Layered Double Hydroxide Electrocatalysts by Tailoring Water Dissociation Active Sites. *Adv. Mater.* **2018**, *30*, 1706279.

(16) Zhao, X.; Wei, H.; Zhao, H.; Wang, Y.; Tang, N. Electrode materials for capacitive deionization: A review. *J. Electroanal. Chem.* **2020**, *873*, 114416.

(17) Pan, Z.; An, J.; Wang, P.; Fan, X.; Shen, T.; Xu, R.; Song, Y.; Song, C. Novel strategy to enhance the desalination performance of flow-electrode capacitive deionization process via the assistance of electro-catalytic water splitting. *Sep. Purif. Technol.* **2021**, *279*, 119753.

(18) Liu, X.; Chi, J.; Dong, B.; Sun, Y. Recent Progress in Decoupled H_2 and O_2 Production from Electrolytic Water Splitting. *ChemElectroChem* **2019**, *6*, 2157−2166.

(19) McHugh, P. J.; Stergiou, A. D.; Symes, M. D. Decoupled Electrochemical Water Splitting: From Fundamentals to Applications. *Adv. Energy Mater.* **2020**, *10*, 2002453.

(20) Landman, A.; Dotan, H.; Shter, G. E.; Wullenkord, M.; Houaijia, A.; Maljusch, A.; Grader, G. S.; Rothschild, A. Photoelectrochemical water splitting in separate oxygen and hydrogen cells. *Nat. Mater.* **2017**, *16*, 646−651.

(21) Ma, Y.; Dong, X.; Wang, Y.; Xia, Y. Decoupling Hydrogen and Oxygen Production in Acidic Water Electrolysis Using a Polytriphenylamine-Based Battery Electrode. *Angew. Chem., Int. Ed.* **2018**, *57*, 2904−2908.

(22) Huang, J.; Xie, Y.; Yan, L.; Wang, B.; Kong, T.; Dong, X.; Wang, Y.; Xia, Y. Decoupled amphoteric water electrolysis and its integration with Mn−Zn battery for flexible utilization of renewables. *Energy Environ. Sci.* **2021**, *14*, 883−889.

(23) Liang, S.; Jiang, M.; Luo, H.; Ma, Y.; Yang, J. A High-Rate Electrode with Grotthuss Topochemistry for Membrane-Free

Decoupled Acid Water Electrolysis. *Adv. Energy Mater.* **2021**, *11*, 2102057.
(24) Zhang, F.; Wang, Q. Redox-Mediated Water Splitting for Decoupled H_2 Production. *ACS Mater. Lett.* **2021**, *3*, 641−651.
(25) Wallace, A. G.; Symes, M. D. Decoupling Strategies in Electrochemical Water Splitting and Beyond. *Joule* **2018**, *2*, 1390−1395.
(26) Landman, A.; Halabi, R.; Dias, P.; Dotan, H.; Mehlmann, A.; Shter, G. E.; Halabi, M.; Naseraldeen, O.; Mendes, A.; Grader, G. S.; et al. Decoupled Photoelectrochemical Water Splitting System for Centralized Hydrogen Production. *Joule* **2020**, *4*, 448−471.
(27) Wang, F.; Sheng, H.; Li, W.; Gerken, J. B.; Jin, S.; Stahl, S. S. Stable Tetrasubstituted Quinone Redox Reservoir for Enhancing Decoupled Hydrogen and Oxygen Evolution. *ACS Energy Lett.* **2021**, *6*, 1533−1539.
(28) Chen, J.; Xiao, R.; Fu, K.; Wu, Y.; Guo, Y.; Yang, S.; Li, H.; Zheng, J.; Li, X. Metal hydride mediated water splitting: Electrical energy saving and decoupled H_2/O_2 generation. *Mater. Today* **2021**, *47*, 16−24.
(29) Rausch, B.; Symes, M. D.; Chisholm, G.; Cronin, L. Decoupled catalytic hydrogen evolution from a molecular metal oxide redox mediator in water splitting. *Science* **2014**, *345*, 1326−1330.
(30) Chen, L.; Dong, X.; Wang, Y.; Xia, Y. Separating hydrogen and oxygen evolution in alkaline water electrolysis using nickel hydroxide. *Nat. Commun.* **2016**, *7*, 11741.
(31) Ma, Y.; Guo, Z.; Dong, X.; Wang, Y.; Xia, Y. Organic Proton-Buffer Electrode to Separate Hydrogen and Oxygen Evolution in Acid Water Electrolysis. *Angew. Chem., Int. Ed.* **2019**, *58*, 4622−4626.
(32) Dotan, H.; Landman, A.; Sheehan, S. W.; Malviya, K. D.; Shter, G. E.; Grave, D. A.; Arzi, Z.; Yehudai, N.; Halabi, M.; Gal, N.; et al. Decoupled hydrogen and oxygen evolution by a two-step electrochemical−chemical cycle for efficient overall water splitting. *Nat. Energy* **2019**, *4*, 786−795.
(33) Landman, A.; Hadash, S.; Shter, G. E.; Ben-Azaria, A.; Dotan, H.; Rothschild, A.; Grader, G. S. High Performance Core/Shell Ni/$Ni(OH)_2$ Electrospun Nanofiber Anodes for Decoupled Water Splitting. *Adv. Funct. Mater.* **2021**, *31*, 2008118.
(34) Wang, Q.; Xu, C. Q.; Liu, W.; Hung, S. F.; Bin Yang, H.; Gao, J.; Cai, W.; Chen, H. M.; Li, J.; Liu, B. Coordination engineering of iridium nanocluster bifunctional electrocatalyst for highly efficient and pH-universal overall water splitting. *Nat. Commun.* **2020**, *11*, 4246.
(35) Chen, J.; Qian, G.; Zhang, H.; Feng, S.; Mo, Y.; Luo, L.; Yin, S. PtCo@PtSn Heterojunction with High Stability/Activity for pH-Universal H_2 Evolution. *Adv. Funct. Mater.* **2022**, 2107597.
(36) Zhu, Z.; Liu, Z.; Yin, Y.; Yuan, Y.; Meng, Y.; Jiang, T.; Peng, Q.; Wang, W.; Chen, W. Production of a hybrid capacitive storage device via hydrogen gas and carbon electrodes coupling. *Nat. Commun.* **2022**, *13*, 2805.
(37) Ruge, M.; Drnec, J.; Rahn, B.; Reikowski, F.; Harrington, D. A.; Carlà, F.; Felici, R.; Stettner, J.; Magnussen, O. M. Structural Reorganization of Pt(111) Electrodes by Electrochemical Oxidation and Reduction. *J. Am. Chem. Soc.* **2017**, *139*, 4532−4539.
(38) Wei, J.-X.; Cao, M.-Z.; Xiao, K.; Guo, X.-P.; Ye, S.-Y.; Liu, Z.-Q. In Situ Confining Pt Clusters in Ultrathin MnO_2 Nanosheets for Highly Efficient Hydrogen Evolution Reaction. *Small Struct.* **2021**, *2*, 2100047.
(39) Wei, J.; Xiao, K.; Chen, Y.; Guo, X.-P.; Huang, B.; Liu, Z.-Q. In situ precise anchoring of Pt single atoms in spinel Mn_3O_4 for a highly efficient hydrogen evolution reaction. *Energy Environ. Sci.* **2022**, *15*, 4592−4600.
(40) Yu, M.; Lu, Y.; Zheng, H.; Lu, X. New Insights into the Operating Voltage of Aqueous Supercapacitors. *Chem. − Eur. J.* **2018**, *24*, 3639−3649.
(41) Sun, W.; Lipka, S. M.; Swartz, C.; Williams, D.; Yang, F. Hemp-derived activated carbons for supercapacitors. *Carbon* **2016**, *103*, 181−192.
(42) Yang, I.; Kwon, D.; Kim, M.-S.; Jung, J. C. A comparative study of activated carbon aerogel and commercial activated carbons as electrode materials for organic electric double-layer capacitors. *Carbon* **2018**, *132*, 503−511.
(43) Yu, L.; Hu, L.; Anasori, B.; Liu, Y.-T.; Zhu, Q.; Zhang, P.; Gogotsi, Y.; Xu, B. MXene-Bonded Activated Carbon as a Flexible Electrode for High-Performance Supercapacitors. *ACS Energy Lett.* **2018**, *3*, 1597−1603.
(44) Xu, Y.; Chang, L.; Hu, Y. H. KOH-assisted microwave post-treatment of activated carbon for efficient symmetrical double-layer capacitors. *Int. J. Energy Res.* **2017**, *41*, 728−735.
(45) Itoi, H.; Maki, S.; Ninomiya, T.; Hasegawa, H.; Matsufusa, H.; Hayashi, S.; Iwata, H.; Ohzawa, Y. Electrochemical polymerization of pyrene and aniline exclusively inside the pores of activated carbon for high-performance asymmetric electrochemical capacitors. *Nanoscale* **2018**, *10*, 9760−9772.
(46) Zhong, M.; Zhang, M.; Li, X. Carbon nanomaterials and their composites for supercapacitors. *Carbon Energy* **2022**, *4*, 950−985.
(47) Hao, S.; Chen, L.; Yu, C.; Yang, B.; Li, Z.; Hou, Y.; Lei, L.; Zhang, X. NiCoMo Hydroxide Nanosheet Arrays Synthesized via Chloride Corrosion for Overall Water Splitting. *ACS Energy Lett.* **2019**, *4*, 952−959.

https://doi.org/10.1021/jacsau.2c00624
JACS Au 2023, 3, 488−497